Triple Frequency GNSS Models for PPP with Float Ambiguity Estimation – Performance Comparison using GPS

Manoj Deo, Ahmed El-Mowafy

Department of Spatial Sciences, Curtin University, Perth, Western Australia

Email: manoj.deo01@gmail.com, Phone: +61 04321 63000

Manoj Deo is currently a Ph.D. candidate at the Department of Spatial Science, Curtin University, Western Australia. He obtained his B.App.Sc and M.Sc degrees in 1998 and 2010, respectively. His current research focus is on precise point positioning with multi-constellation and multi-frequency GNSS.

Ahmed El-Mowafy is Associate Professor at the Department of Spatial Sciences, Curtin University, Western Australia. He has obtained his Ph.D. from the University of Calgary, Canada, in 1995. He has extensive publications in precise positioning and navigation using GNSS, quality control and integrity monitoring, estimation theory, and attitude determination.

Triple Frequency GNSS Models for PPP with Float Ambiguity Estimation – Performance Comparison using GPS

Abstract

Although precise point positioning (PPP) is a well-established technique, it requires a significant convergence time of 30 minutes or more to reach an accuracy of a few cm. The availability of triple-frequency measurements from modernised GPS as well as other GNSS constellations provides an opportunity to formulate new models that provide better performance than the widely used dual-frequency ionosphere-free PPP model.

This contribution proposes two new PPP models that use triple-frequency data, which were designed to accelerate convergence of carrier phase float ambiguities. The first model uses a triple-frequency ionosphere-free linear combination that has minimum noise propagation and geometry preserving properties. The second model uses a mixed code and carrier phase linear combination with the same properties. A third model was also implemented, which uses individual uncombined triple-frequency measurements.

The three models were validated using triple-frequency GPS data and their performance was compared to the traditional dual-frequency model in terms of the convergence time taken to achieve and maintain a uniform 3-dimensional accuracy of 5cm. Testing includes PPP processing of 1-hour measurement blocks using 1-8 days of data from three locations in Australia. It was shown that all the three triple-frequency models had improved solution convergence time compared to the traditional PPP dual-frequency model although they almost gave similar accuracy and precision. The convergence time when using the triple-frequency ionosphere-free model improved by 10%, the improvement was 9% when using the mixed code-phase model whereas the individual uncombined model resulted in 8% improvement. These results show the significance of the triple frequency observations for future PPP applications.

Keywords: Precise point positioning, convergence, linear combinations, multi-frequency, GNSS.

Introduction

Precise point positioning (PPP) (Zumberge *et al*., 1997) is a well-established technique for achieving cm to sub-decimetre level positioning accuracy using a standalone GNSS receiver. It is used in various applications such as deformation monitoring, volcanic monitoring, and crustal motion studies. However, one concern in PPP is its need for a lengthy period, typically 30 minutes under normal conditions, to reduce the impact of the code noise such that the float ambiguities converge and give a solution better than a decimetre level of accuracy. This presents a major problem for many real-time applications that require the convergence to occur quickly prior to commencing the actual positioning. The solution convergence depends on several factors such as number of satellites observed (redundancy), satellite geometry, multipath, atmospheric effects (troposphere, ionosphere) and the level of pseudorange noise, which is magnified when using the ionosphere-free combination. In addition, PPP errors may vary from day to day at the same site, despite the GPS constellation repeating itself almost every 12 hours (Bisnath and Gao, 2009). A number of research efforts have been made to reduce PPP convergence time to make it more practical. Gao and Shen (2002) introduced a mixed code-phase ionosphere-free linear combination that showed marginal improvements in convergence time. Ge *et al*. (2008) presented a PPP method with integer ambiguity

resolution (PPP-AR), which was further refined in Geng *et al*. (2010). PPP-AR typically involves three steps; 1) estimation of reliable float ambiguities, 2) solving integer ambiguities, and 3) validating the integer solution. The receiver fractional phase biases are removed by performing between-satellite-single differencing (BSSD). Some PPP-AR methods estimate or use calibrated values of the satellite non-integer fractional phase biases, also known as fractional cycle biases (FCBs). Other PPP-AR methods have been proposed such as the integer-recovery clock method (Laurichesse *et al*., 2009) and the decoupled clock model (Collins *et al*., 2010). However, the convergence time in these ambiguity fixing PPP algorithms using dual-frequency measurements still remains to be around 30 minutes. The stabilisation and quick convergence of float ambiguities is a crucial first step for PPP-AR as well as conventional PPP.

The availability of triple-frequency measurements from modernised GPS Block IIF satellites, BeiDou and Galileo as well as other regional systems such as QZSS, provides an opportunity to improve the performance of PPP. For example, Geng and Bock (2013) presented a PPP-AR method designed for rapid ambiguity resolution using triple-frequency data. The method was based on the strategy used in Ge *et al*. (2008) and Geng *et al*. (2010), and commences with solving the L2/L5 extra wide-lane ambiguity using Melbourne-Wübbena linear combination, instead of the L1/L2 wide-lane ambiguity used in former studies. This is followed by solving an ionosphere-free wide-lane ambiguity, and subsequently the narrow-lane ambiguities. Continuously operating reference station (CORS) network data is required to solve for the fractional phase biases, and the authors claimed wide-lane and narrow-lane ambiguity correctness rate of 99% in 20s and 65s, respectively. The study was based on simulated triple-frequency GPS data and the model did not consider treatment of initial fractional phase biases, which must be corrected prior to ambiguity fixing. As a refinement to conventional PPP, Banville *et al*. (2014) used global and regional ionospheric corrections, together with satellite phase biases for reducing the convergence time. However, users of this method must use specific ionospheric corrections that are compatible with this methodology. Seepersad and Bisnath (2014) focused on code noise and multipath reduction to improve convergence, reporting a 34% improvement. Shi *et al.* (2014) proposed local troposphere model to augment real-time PPP where data from a CORS network was used to estimate the Zenith Wet Delay (ZWD) at each station. This was modelled with optimal fitting coefficients and broadcast to users where decimetre accuracy was achieved within an improved 20 mins, which shows that the PPP model is strengthened if external information is provided on the troposphere.

Recent research interest has also being focussed on development of suitable linear combinations for PPP. Henkel and Günther (2008) discussed triple-frequency low noise code-phase linear combinations that are suitable for estimating integer ambiguities in PPP. Elsobeiey (2015) compared nine triple-frequency linear combinations to study improvements in PPP convergence time and precision using GPS. However, no mathematical background was provided in the derivation of these linear combinations and the linear combination that was found to give best performance for GPS L1, L2 and L5 had the coefficients 2.7018, -2.1053, 0.4035, which give a significant noise propagation of 3.85 and is not completely ionosphere-free (ionospheric content was -0.0419 of the delay in L1). Also, the analysis did not consider anomalies in the L5 carrier phase measurements due to thermal variations at the satellite (Montenbruck *et al*., 2012; Tegedor & Øvstedal, 2014), and there were only two Block IIF satellites that were simultaneously tracked in the dataset for that study.

This contribution proposes two new linear combinations to improve convergence time of the dual-frequency ionosphere-free combinations used in conventional PPP by utilising triple-frequency data. These combinations are:

(1) Ionosphere-free, geometry preserving triple-frequency linear combination of phase-only or code-only measurements that has lowest noise propagation.

(2) A mixed code and phase linear combination that also has the above properties, which is an extension of the approach taken in Gao and Shen (2002) by considering a third frequency to further reduce the code noise.

It is hypothesised that minimising the pseudorange noise while keeping the measurements ionosphere-free would give optimum results. The first part of this paper presents triple-frequency observation equations, followed by derivation of the two new linear combinations. Another PPP model is also tested, which uses individual un-combined signals. Simulated GPS data is used to evaluate the performance of these models in terms of convergence time and accuracy compared with the standard L1/L2 dual-frequency traditional PPP solutions. Finally, the results are discussed and conclusions are presented.

Observation Equations

The observation equations for the triple-frequency pseudorange and carrier-phase measurements (scaled to distance units), for satellite k from a GNSS constellation, such as GPS (denoted here as G), to receiver r are:

$$P(i)_r^{k_G} = \rho_r^{k_G} + c\big(dt_{r_G} - dt^{k_G} + d(i)_{r_G} + d(i)^{k_G}\big) + T^{k_G} + \mu_i\, I^{k_G} + \varepsilon_{P(i)_r}^{k_G} \tag{1}$$

$$\phi(i)_r^{k_G} = \rho_r^{k_G} + c\big(dt_{r_G} - dt^{k_G}\big) + T^{k_G} - \mu_i\, I^{k_G} + \lambda_1\big(N(i)_r^{k_G} + \delta(i)_{r_G} + \delta(i)^{k_G}\big) + \varepsilon_{\phi(i)_r}^{k_G} \tag{2}$$

where i is the frequency identifier, such that i= 1, 2, 5 for GPS L1, L2 and L5, respectively as an example; $P(i)$ and $\phi(i)$ are the pseudorange and carrier-phase measurements whereas frequency is denoted as f_i. ρ is the satellite-to-receiver geometric range; c is the speed of light in vacuum; dt_{r_G} and dt^{k_G} are the receiver and satellite clock offsets for GPS, where the latter is eliminated in PPP by the use of precise clock corrections. It is noted here that the International GNSS Service (IGS) precise clock corrections are modelled for L1/L2 ionosphere-free combinations and biases must be considered when using individual signals or other linear combinations as shown in El-Mowafy et al. (2016). T^{k_G} is the tropospheric delay; λ_i denotes the wavelength for frequency i. $\mu_i = \frac{f_1^2}{f_i^2}$ is the dispersive coefficient and I^{k_G} is the ionosphere error for a reference frequency, e.g. L1 for GPS. $\varepsilon_{\phi(i)_r}^{k_G}$ includes measurement noise and multipath of the carrier-phase measurement whereas $\varepsilon_{P(i)_r}^{k_G}$ denotes code measurement noise and multipath. $d(i)_{r_G}$ is the receiver hardware bias for code measurement for frequency i, $d(i)^{k_G}$ is the satellite hardware bias. The IGS satellite clock offsets are determined from ionosphere-free measurements with embedded P1 and P2 Differential Code Biases (DCBs). $d(i)^{k_G}$ includes the additional satellite DCBs if using signals other than the reference signals P1 and P2, triple-frequency combinations or individual uncombined in the PPP model. These DCBs are available as an IGS Multi-GNSS Experiment (MGEX) product (Montenbruck et al., 2014). The receiver dependent code hardware delays remain in the equations. $N(i)_r^{k_G}$ is the integer ambiguity term whereas $\delta(i)_{r_G}$ and $\delta(i)^{k_G}$ are the receiver and satellite hardware biases for the carrier-phase measurements, respectively, which make the ambiguity a non-integer term (Shi and Gao, 2014). One strategy to deal with the receiver clock and hardware biases is to apply the BSSD model, which removes common receiver related biases for both pseudorange and phase signals from the same frequencies of the same constellation (El-Mowafy et al., 2016). Another approach is to lump the receiver biases with other unknowns such as clock offsets, for individual constellations and estimate it as part of the inter-system biases (El-Mowafy et al., 2016).

Modelling different types of biases in the uncombined form presents additional complexities because they have the same coefficients in the solution design matrix, resulting in rank deficiency and inability to separate them. The preferred approach for satellite biases is to estimate them externally and provide them to users as "calibration" quantities. Alternatively, when solving float ambiguities, the biases may be lumped with the phase ambiguity terms and considered to be constant during the observation period since the biases are usually stable over several hours. Assuming that all biases except for the initial fraction phase biases have been accounted for by any of these approaches, BSSD measurements are used and the IGS precise clock corrections are applied, the observation Eq. 1 and 2 are simplified to:

$$P(i) = \rho + \mu_i I + T + \varepsilon_{P(i)} \tag{3}$$

$$\phi(i) = \rho - \mu_i I + \lambda_1 N(i)^* + T + \varepsilon_{\phi(i)} \tag{4}$$

where $N(i)^*$ is real numbers that includes the integer ambiguities and observation biases. The system and receiver identifiers have been removed when we are dealing with measurements from one constellation and since only a single receiver is considered in PPP. However, one should note that integration of multi-constellation data introduces additional biases such as inter-system bias, constellation and receiver time offsets and DCBs. Dealing with these biases is beyond the scope of this paper and a comprehensive discussion on their source, modelling and treatment is given in our earlier work in El-Mowafy et al. (2016).

PPP Using Triple Frequency Observations
In this section we introduce the proposed models using the triple frequency data.

The use of individual uncombined signals

The individual uncombined multi-frequency GNSS measurements can form the PPP model. Such a model avoids noise propagation by not creating linear combinations of observations. Thus, Eq. 3 and 4 are used for the code and phase measurements for each frequency (e.g. L1, L2 and L5 for GPS). The ionospheric bias is estimated using the third frequency measurement rather than forming ionosphere-free combinations. The unknown parameters include three position parameters and a troposphere Zenith Wet Delay (ZWD) parameter, which is assumed common to all satellite measurements and is modelled by applying a wet troposphere mapping function to map the ZWD to the slant receiver-satellite line of sight. The hydrostatic troposphere delay is modelled using an empirical model (Tuka and El-Mowafy, 2013). Each satellite introduces a slant ionosphere delay and three ambiguity parameters. If BSSD is not used, there is also an additional receiver clock offset parameter.

Low noise, ionosphere-free, geometry preserving triple-frequency phase-only and code-only linear combination

This section proposes a PPP model which uses a triple-frequency linear combination that is ionosphere-free, geometry preserving and has lowest noise propagation, designed for faster ambiguity convergence compared to the traditional dual-frequency model. Concurrently with our study, Guo et al. (2016) presented a similar approach for BeiDou only observations where only approximate values of the model coefficients were given. In our study, the derivation of the combination coefficients for all constellations including GPS, QZSS, Galileo, BeiDou and the proposed GLONASS K2 Code Division Multiple Access (CDMA) signals are given (Yuri et al.,

2011). This triple-frequency linear combination is applied to both carrier-phase and code measurements. A linear combination of triple-frequency phase measurements, where the frequencies are denoted in general as f_1, f_2 and f_3, is given as (Cocard et $al.$, 2008):

$$P = \alpha_1 P1 + \alpha_2 P2 + \alpha_3 P3 \tag{5}$$

$$\phi = \alpha_1 \phi1 + \alpha_2 \phi2 + \alpha_3 \phi3 \tag{6}$$

where α_1, α_2 and α_3 are the linear combination coefficients for the three-frequency measurements. The geometry preservation condition is achieved by:

$$\alpha_1 + \alpha_2 + \alpha_3 = 1 \tag{7}$$

The first order ionosphere-free condition, which contains the majority of the ionospheric effect, is removed when:

$$\frac{\alpha_1 \cdot 40.3 TEC}{f_1^2} + \frac{\alpha_2 \cdot 40.3 TEC}{f_2^2} + \frac{\alpha_3 \cdot 40.3 TEC}{f_3^2} = 0 \tag{8}$$

The carrier frequencies are expressed in terms of a base GNSS frequency f_0, such that $f_j = \sqrt{k_j} f_0$, where f_0 is 10.23MHz, and $\sqrt{k_j}$ is the frequency multiplier. The frequency multipliers for GPS, QZSS, Galileo, BeiDou and the proposed GLONASS K2 CDMA are given in Table 1. Accordingly, Eq. 8 can be simplified to:

$$\frac{\alpha_1}{k_1} + \frac{\alpha_2}{k_2} + \frac{\alpha_3}{k_3} = 0 \tag{9}$$

Table 1: Multi-constellation GNSS frequencies and frequency multipliers of a base frequency 10.23 Mhz.

GNSS Constellation	Signal	Frequency Multiplier ($\sqrt{k}$)
GPS/ QZSS	L1	154
	L2	120
	L5	115
	LEX (QZSS only)	125
Galileo	E1	154
	E5a	115
	E5b	118
	E5(a+b)	116.5
	E6	125
BeiDou	B1	152.6
	B2	118
	B3	124
GLONASS K2(CDMA)	L1	156.5
	L2	122
	L3	117.5

Richert and El-Sheimy (2007) suggested that many coefficents can satisfy the above two criteria given in (Eq. 7 and 9). However, the dual-frequency ionosphere-free observation combination used in the traditional PPP model has a high noise amplification factor $\epsilon =$

$\sqrt{\alpha_1^2 + \alpha_2^2} = 2.978$ for L1-L2 measurements for example. In this study, we use the measurement from a third frequency to form a separate condition that results in a minimum noise propagation. In a simplified form, assuming that the noise is the same for phase measurements on all frequencies, the noise propagation is directly proportional to $\sigma_\phi^2 = \sigma_{\phi j}^2 (\alpha_1^2 + \alpha_2^2 + \alpha_3^2) = \sigma_{\phi j}^2 \epsilon^2$. Hence, the noise amplification factor is minimised by the condition:

$$(\alpha_1^2 + \alpha_2^2 + \alpha_3^2) = \epsilon^2 = MIN \tag{10}$$

Satisfying the above three conditions (Eq. 7, 9, and 10) would result in a linear combination with the potential to reduce PPP solution convergence time and improve positional accuracy. A solution for α_1, α_2 and α_3, from Eq. 7, 9 and 10 is now derived algebraically. Rearranging Eq. 7 as $\alpha_1 = 1 - \alpha_2 - \alpha_3$, substituting into Eq. 9 and rearranging in terms of α_2 results in:

$$\alpha_2 = \frac{\alpha_3(k_2 k_3 - k_1 k_2) - k_2 k_3}{k_1 k_3 - k_2 k_3} \tag{11}$$

and

$$\alpha_2^2 = \frac{\alpha_3^2(k_2 k_3 - k_1 k_2)^2 - 2\alpha_3 k_2 k_3(k_2 k_3 - k_1 k_2) + (k_2 k_3)^2}{k_3^2(k_1 - k_2)^2} \tag{12}$$

Substituting Eq. 11 into 7 and rearranging in terms of α_1 gives

$$\alpha_1 = \frac{\alpha_3(k_1 k_2 - k_1 k_3) - k_1 k_3}{k_1 k_3 - k_2 k_3} \tag{13}$$

and

$$\alpha_1^2 = \frac{\alpha_3^2(k_1 k_2 - k_1 k_3)^2 - 2\alpha_3 k_1 k_3(k_1 k_2 - k_1 k_3) + (k_1 k_3)^2}{k_3^2(k_1 - k_2)^2} \tag{14}$$

Substituting Eq. 12 and 14 into 10 results in a quadratic equation of the form:

$$A\alpha_3^2 + B\alpha_3 + C = 0 \tag{15}$$

where the constants A, B and C are:

$$A = (k_1 k_2 - k_1 k_3)^2 + (k_2 k_3 - k_1 k_2)^2 + (k_1 k_3 - k_2 k_3)^2 \tag{16}$$

$$B = 2k_1 k_3(k_1 k_2 - k_1 k_3) - 2k_2 k_3(k_2 k_3 - k_1 k_2) \tag{17}$$

$$C = (k_1 k_3)^2 + (k_2 k_3)^2 - \epsilon^2(k_1 k_3 - k_2 k_3)^2 \tag{2}$$

The quantities A and B are constants whereas C contains an unknown value for the noise amplification factor ϵ. There are two unknown variables α_3 and ϵ, in these equations, and the discriminant $B^2 - 4AC$ should be greater than zero for a real value solution for α_3. Furthermore, the noise amplification factor is minimized when the discriminant is exactly zero, resulting in only one real root. C is obtained by:

$$C = \frac{B^2}{4A} \tag{19}$$

From Eq. 15, a solution for α_3 is obtained as follows:

$$\alpha_3 = \frac{-B}{2A} = \frac{-q}{A} = \frac{C}{q} \tag{20}$$

where $q = -0.5B$. The value of α_3 is substituted into Eq. 11 and 7 to solve for α_2 and α_1, respectively. These coefficients for the triple-frequency linear combination α_1, α_2 and α_3, are given in Table 2 for GPS, QZSS, Galileo, BeiDou and GLONASS K2 CDMA signals, based on the frequency multiplier values given in Table 1. Also given in Table 2 are the values for the noise amplification factor, ϵ, calculated as:

$$\epsilon = \sqrt{\frac{(k_1 k_3)^4 + (k_2 k_3)^4 - C}{\left(k_1^2 k_3^2 - k_2^2 k_3^2\right)^2}} \tag{21}$$

Table 2 additionally shows the percentage change in noise when using the given triple-frequency combinations with values of α_1, α_2 and α_3 from the proposed ionosphere-free combination, compared to the ionosphere-free dual-frequency combinations that are used for generating precise clock corrections by the IGS. These reference signals are L1/L2 for GPS, B1/B2 for BeiDou (Zhao *et al*., 2013) and E1/E5a for Galileo (Prange *et al*., 2012; Uhlemann *et al*., 2012). For GLONASS K2, the L1/L2 CDMA signals are assumed as the reference signals. A significant noise reduction is obtained using the proposed method at 14% for GPS, 3.1% for Galileo, 1.1% for BeiDou and 13.6% for GLONASS K2.

Table 2: Coefficients for triple-frequency linear combinations for different GNSS constellations and signals, with percentage change in noise compared to dual-frequency reference signals. For GLONASS K2, the L1/L2 CDMA signals are assumed as the reference signals.

GNSS Constellation	Signal Combination	α_1	α_2	α_3	Noise Amp. Factor (ϵ)	Percentage change
GPS	L1-L2-L5	2.326 944	-0.359 646	-0.967 299	2.546	-14.5%
QZSS	L1-LEX-L5	2.269 122	-0.024 529	-1.244 592	2.588	-13.1%
Galileo	E1-E5a-E5b	2.314 925	-0.836 269	-0.478 656	2.507	-3.1%
BeiDou	B1-B3-B2	2.566 439	-0.337 510	-1.228 930	2.865	-1.1%
GLONASS K2 (CDMA)	L1-L2-L3	2.359 142	-0.404 596	-0.954 546	2.577	-13.6%

A refined dual-frequency mixed code-carrier PPP model

The previous section presented a triple-frequency combination for carrier phase and code observations separately. In this section, a mixed code-carrier phase linear combination is formed that is ionosphere-free, geometry preserving and has minimum noise propagation. This PPP model is built from linear combinations of two dual-frequencies such as L1/L2 and L1/L5 for GPS, as well as the carrier-phase only dual-frequency ionosphere-free combinations for the same frequencies to complete the model. This model solves for the individual non-integer carrier-phase ambiguities for each frequency (i.e. $N1^*, N2^*$ and $N5^*$ for GPS) as well as the receiver position and troposphere error. Using a pair of code and carrier-phase measurements of frequencies from the same GNSS constellation, e.g. L1 and L2 GPS, the mixed code-carrier phase combination is expressed as:

$$\theta 12 = \alpha_1 \phi 1 + \alpha_2 \phi 2 + \beta_1 P1 + \beta_2 P2 \tag{3}$$

where α_1 and α_2 are the coefficients for the carrier-phase measurements and β_1 and β_2 are the coefficients for the code measurements. The ionosphere-free condition is formed by:

$$40.3 TEC \left[\frac{-\alpha_1}{f_1^2} + \frac{-\alpha_2}{f_2^2} + \frac{\beta_1}{f_1^2} + \frac{\beta_2}{f_2^2} \right] = 0 \tag{23}$$

and the geometry preserving condition is:

$$\alpha_1 + \alpha_2 + \beta_1 + \beta_2 = 1 \tag{24}$$

Let us assume that the code noise is higher than the phase noise by a factor, a, e.g. $a = 100$ for GPS, and the noise for carrier-phase measurements on all its frequencies is the same, i.e., $\sigma_\phi = \sigma_{\phi 1} = \sigma_{\phi 2}$. The noise in the combination is minimised by minimising the amplification factors by using the following condition:

$$\alpha_1^2 + \alpha_2^2 + a^2 \beta_1^2 + a^2 \beta_2^2 = \epsilon^2 = MIN \tag{25}$$

The code and carrier-phase measurements are now weighted according to their measurement noise. A solution that satisfies the above three conditions will give the required coefficients α_1, α_2, β_1 and β_2 for the mixed code-carrier linear combination. The derivation of these coefficients is given in Appendix A for the interested reader.

Table 3 shows the derived coefficients α_1, α_2, β_1 and β_2, as well as the noise amplification factor ϵ for GPS, QZSS, Galileo, GLONASS K2 and BeiDou. The actual noise in the combination, in distance units, is evaluated by $\epsilon \sigma_\phi$, where σ_ϕ is the carrier-phase noise, typically a few millimetres for GPS. As shown in the table, the contribution of code measurement noise is supressed in the mixed code-phase combinations, since the absolute values of their coefficients are much smaller than the carrier-phase coefficients. Note here that since the code coefficients are multiplied by pseudoranges, which are large values in thousands of kilometres; thus, the linear combination value is significant and is numerically stable. As an example, if we assume the phase noise is $\sigma_\phi = 0.002m$ and the corresponding code noise is $\sigma_P = 0.2m$ for GPS L1 and L2, the total noise in the proposed mixed code-phase combination is just $0.006m$.

For the triple-frequency code and phase measurements, there would be only two independent mixed code-phase combinations. Considering GPS as an example, the mixed code-phase combinations L1/L2 and L1/L5 may be used in the same model. These two mixed code-phase combinations are used with the corresponding carrier phase only dual-frequency ionosphere-free combinations L1/L2 and L1/L5 to complete the mixed code-phase PPP model. This model will have correlations between the linear combinations used, which will be discussed in a later section.

Table 3: Coefficients for mixed code-carrier phase linear combinations with measurement noise (m), using $\sigma_P = 0.2m$ and $\sigma_\phi = 0.002m$.

GNSS Constellation	Signal Combination	α_1	α_2	β_1	β_2	ϵ	Noise (m)
GPS	L1-L2	2.529802	-1.533226	0.001509	0.001915	2.968	0.006
GPS	L1-L5	2.250109	-1.252675	0.001108	0.001458	2.582	0.005
GPS	L2-L5	10.078988	-9.169588	0.044338	0.046263	15.057	0.030
QZSS	L1-LEX	2.905273	-1.910056	0.002150	0.002632	3.493	0.007
QZSS	LEX-L2	10.329707	-9.426643	0.047481	0.049456	15.575	0.031
QZSS	LEX-L5	6.166649	-5.194059	0.013137	0.014273	8.293	0.017
BeiDou	B1-B2	2.472483	-1.475721	0.001422	0.001816	2.889	0.006
BeiDou	B1-B3	2.917418	-1.922248	0.002173	0.002657	3.511	0.007
BeiDou	B2-B3	-8.209041	9.138934	0.035920	0.034186	13.248	0.026
Galileo	E1-E5a	2.250109	-1.252675	0.001108	0.001458	2.582	0.005
Galileo	E1-E5b	2.408595	-1.411632	0.001327	0.001709	2.800	0.006
Galileo	E5a-E5b	-11.70299	12.514784	0.095313	0.092891	21.696	0.043
GLONASS K2	L1-L2	2.533086	-1.536521	0.001514	0.001921	2.973	0.006
GLONASS K2	L1-L3	2.280974	-1.283628	0.001149	0.001506	2.624	0.005
GLONASS K2	L2-L3	10.812700	-9.923189	0.054208	0.056281	16.627	0.033

Summary of PPP models

Table **4** summarises the presented PPP models compared to the traditional dual-frequency PPP model in terms of the observation equations, number of observations, unknown parameters and their descriptions. The BSSD approach is used where one satellite is taken as a pivot and measurements from the remaining satellites are differenced with its measurements. All the presented triple-frequency models require a minimum of five satellites. The troposphere term is separated into a zenith hydrostatic component and a wet component, with the use of a mapping function such as the Vienna Mapping Function (VMF) (Bohem et al., 2006) to map the slant delays to the zenith direction. The zenith hydrostatic delay is modelled using an empirical model, such as Saastamoinen (Davis et al., 1985). The unknown parameters include three position parameters and ZWD, which are common in all model equations. There are $n-1$ ambiguities to resolve for each carrier phase combination in the triple-frequency ionosphere-free model. For the mixed code-phase and individual uncombined models, the ambiguities are resolved for each frequency; thus there are $3(n-1)$ ambiguities to resolve. Although it may appear that a solution is possible with four satellites for the individual uncombined model, the two extra measurements of the third frequency do not add to the required geometry of the observed satellites, thus five satellites are still needed to form four single differences for eliminating the receiver clock offset and estimating the three position components and ZWD. Although the three different models differ in their functional model, they are expected to give similar performance since they all provide the same observations.

Table 4: Summary of PPP models being compared, the first three rows include three code and three phase observations.

PPP Model	Primary model equations	Number of obs for n satellites	Number of unknowns	Parameter description
Individual Uncombined Signals	$\phi1, \phi2, \phi5$ $P1, P2, P5$ (Eqs. 3, 4)	$6(n-1)$ $= 6n - 6$	$4 + 4(n-1)$ $= 4n$	$X, Y, Z, ZWD,$ $(n-1)\{I, N1^*, N2^*, N5^*\}$
Triple-frequency ionosphere-free	ϕ, P (Eqs. 5, 6)	$2(n-1)$ $= 2n - 2$	$4 + (n-1)$ $= 3 + n$	$X, Y, Z, ZWD,$ $(n-1)\{N^*\}$
Mixed code-phase	$\phi12, \phi15$ $\Theta12, \Theta15,$ (Eq. 22)	$4(n-1)$ $= 4n - 4$	$4 + 3(n-1)$ $= 1 + 3n$	$X, Y, Z, ZWD,$ $(n-1)\{N1^*, N2^*, N5^*\}$
Traditional Dual-frequency ionosphere-free	$\phi12, P12$	$2(n-1)$ $= 2n - 2$	$4 + (n-1)$ $= 3 + n$	$X, Y, Z, ZWD,$ $(n-1)\{N^*\}$

Stochastic modelling of the observations

The satellite elevation-dependent weighting scheme is applied and the variance matrix of the individual measurements model for GPS as an example is

$$Q = diag\begin{bmatrix} \sigma^2_{\phi_1} & \sigma^2_{\phi_2} & \sigma^2_{\phi_5} & \sigma^2_{P_1} & \sigma^2_{P_2} & \sigma^2_{P_5} \end{bmatrix} \tag{26}$$

with off-diagonal terms zero where no-correlation is assumed among the individual observations at each epoch. The values for standard deviations can be estimated and validated as shown in El-Mowafy (2014; 2015). For the low noise triple frequency ionosphere free model, the covariance matrix is evaluated with the error propagation law as

$$Q_l = DQD^T \tag{27}$$

where

$$D = \begin{bmatrix} \frac{\partial \phi}{\partial \phi_1} & \frac{\partial \phi}{\partial \phi_2} & \frac{\partial \phi}{\partial \phi_5} & \frac{\partial \phi}{\partial P_1} & \frac{\partial \phi}{\partial P_2} & \frac{\partial \phi}{\partial P_5} \\ \frac{\partial P}{\partial \phi_1} & \frac{\partial P}{\partial \phi_2} & \frac{\partial P}{\partial \phi_5} & \frac{\partial P}{\partial P_1} & \frac{\partial P}{\partial P_2} & \frac{\partial P}{\partial P_5} \end{bmatrix} = \begin{bmatrix} \alpha_1 & \alpha_2 & \alpha_3 & 0 & 0 & 0 \\ 0 & 0 & 0 & \alpha_1 & \alpha_2 & \alpha_3 \end{bmatrix} \tag{28}$$

where ϕ and P are defined in Eqs. 5 and 6. The matrix Q_l results in a diagonal matrix with off-diagonal terms as zero, indicating the linear combinations used in the model are uncorrelated. For the mixed code-phase model, the D matrix reads

$$D = \begin{bmatrix} \dfrac{\partial \phi_{12}}{\partial \phi_1} & \dfrac{\partial \phi_{12}}{\partial \phi_2} & \dfrac{\partial \phi_{12}}{\partial \phi_5} & \dfrac{\partial \phi_{12}}{\partial P_1} & \dfrac{\partial \phi_{12}}{\partial P_2} & \dfrac{\partial \phi_{12}}{\partial P_5} \\[2mm] \dfrac{\partial \phi_{15}}{\partial \phi_1} & \dfrac{\partial \phi_{15}}{\partial \phi_2} & \dfrac{\partial \phi_{15}}{\partial \phi_5} & \dfrac{\partial \phi_{15}}{\partial P_1} & \dfrac{\partial \phi_{15}}{\partial P_2} & \dfrac{\partial \phi_{15}}{\partial P_5} \\[2mm] \dfrac{\partial \Theta_{12}}{\partial \phi_1} & \dfrac{\partial \Theta_{12}}{\partial \phi_2} & \dfrac{\partial \Theta_{12}}{\partial \phi_5} & \dfrac{\partial \Theta_{12}}{\partial P_1} & \dfrac{\partial \Theta_{12}}{\partial P_2} & \dfrac{\partial \Theta_{12}}{\partial P_5} \\[2mm] \dfrac{\partial \Theta_{15}}{\partial \phi_1} & \dfrac{\partial \Theta_{15}}{\partial \phi_2} & \dfrac{\partial \Theta_{15}}{\partial \phi_5} & \dfrac{\partial \Theta_{15}}{\partial P_1} & \dfrac{\partial \Theta_{15}}{\partial P_2} & \dfrac{\partial \Theta_{15}}{\partial P_5} \end{bmatrix} = \begin{bmatrix} \dfrac{f_1^2}{f_1^2-f_2^2} & \dfrac{-f_2^2}{f_1^2-f_2^2} & 0 & 0 & 0 & 0 \\[2mm] \dfrac{f_1^2}{f_1^2-f_5^2} & 0 & \dfrac{-f_5^2}{f_1^2-f_5^2} & 0 & 0 & 0 \\[2mm] \alpha_{1(1,2)} & \alpha_{2(1,2)} & 0 & \beta_{1(1,2)} & \beta_{2(1,2)} & 0 \\[2mm] \alpha_{1(1,5)} & 0 & \alpha_{2(1,5)} & \beta_{1(1,5)} & 0 & \beta_{2(1,5)} \end{bmatrix}$$

(29)

and the measurement covariance matrix is computed using Eq. 27, resulting in a fully populated matrix.

As an example, assuming uncorrelated raw phase and code measurements with $\sigma_{\phi_1} = \sigma_{\phi_2} = \sigma_{\phi_5} = 0.002m$ and $\sigma_{P_1} = \sigma_{P_2} = \sigma_{P_5} = 0.2m$; The measurement covariance matrix computed at the zenith is

$$Q_y = \begin{bmatrix} 3.55 & 2.30 & 3.52 & 2.29 \\ 2.30 & 2.68 & 2.29 & 2.67 \\ 3.52 & 2.29 & 3.52 & 2.28 \\ 2.29 & 2.67 & 2.28 & 2.67 \end{bmatrix}^{\times 10^{-5}}$$

(30)

which gives correlation between observations reaching above 0.7. This indicates that the correlations between the linear combinations used in this model must be considered in the stochastic modelling of the observations.

Validation of the Presented PPP Models

This section compares the performance of the presented PPP models, commencing with a description of the data used and followed by validation of the models. The validation process uses GPS as an example, where it equally applies to any single GNSS constellation.

Test Description

Triple-frequency GPS static data from three Australian continuously operating GNSS stations, HOB2, TIDB and CEDU was used to test the proposed PPP models. The measurement modelling and simulation were carried out with the following approach:

i. The following IGS products were used: final precise ephemeris; IGS satellite clock product for satellite clock error, dt^{k_G}; IGS ZTD product for the troposphere; and the broadcast Klobuchar model for the ionospheric delay. IGS produces ZTD and station receiver clock products for selected IGS stations using standard PPP, which were used to estimate realistic errors in the simulated data.

ii. The satellite and receiver DCBs were ignored. Inter-system biases are not applicable in this case because a single constellation is used where all satellites are transmitting measurements on the same frequencies.

iii. Measurement noise was generated assuming it has a normal distribution with zero mean and standard deviation of 0.4m for code and 0.01 cycles for carrier phase. A satellite elevation mask angle of 10 degrees was used.

The accuracy of PPP results was assessed by referencing them to the known stations precise coordinates that were obtained from the Asia Pacific Reference Frame (APREF) project records. The

period of data analysed per station was 8 days at HOB2, 6 days at TIDB, and 1 day at CEDU, with a sampling interval of 15 s. The data was processed in hourly blocks, with the ambiguities re-initialised at the start of each hour.

Analysis and Discussion of Results

The three proposed PPP models were implemented using Kalman filter processing. Results are compared in terms of solution convergence time, accuracy and precision where the convergence time is defined as the time when a 3-dimentional (3D) positional accuracy of 0.05m is reached and maintained thereafter. This accuracy is targeted towards the surveying and high precision industry sector, which accounts for 23.3% of the GNSS market users where 47.8% of this sector requires accuracy within 1-5cm (GPS World, 2016). The accuracy is defined as the root mean squared errors (RMSE) after convergence is achieved with respect to the known station position.

The mean convergence times and RMSE (in East, North, Up) from PPP analysis for the four algorithms are shown in Table 5. Compared to the dual-frequency traditional PPP model, the convergence time for the triple-frequency ionosphere-free model improved by 11% (3.1 min), the mixed code phase model improved by 9% (2.6 min) whereas the individual signal model improved by 8% (2.4 min). The accuracy results given in columns 3-5 represent the solutions that converged within 5cm 3D positioning accuracy in less than one hour. The change in the RMSE in East, North and Up directions were insignificant (at or below 1mm) for all the three PPP models, which indicate that they gave the same positioning accuracy. This is expected since although the three different triple frequency models differ in their functional model and parameterizations, they have the same information content; i.e. use of triple frequency phase and code data with the same precise orbit and clock correction products.

The individual uncombined model has no noise propagation, but this did not markedly improve its performance compared to the other triple frequency models due to considering this amplification in the observation covariance and weights. Further testing was done to investigate whether estimation of the extra ionospheric parameter by processing a days' simulated GPS data firstly by estimating the ionosphere error as an unknown PPP parameter, and secondly removing it by applying an ionosphere model (the known Klobuchar's model). The mean convergence time for the 24-hourly solutions was 26.7 minutes when estimating the ionospheric error, whereas it was reduced to only 9.4 minutes when the ionosphere delay was eliminated assuming that is provided externally. This indicates that using the individual uncombined model with ionosphere augmentation will significantly improve convergence time.

Table 5: Mean RMSE (East, North and Up) and convergence time for the GPS PPP algorithms tested with hourly data sessions. Columns 3-5 present statistics for solutions that converged within 3D accuracy of 5cm in less than 1 hour.

PPP Model	Mean Convergence Time (min)	Mean RMSE - East Converged (m)	Mean RMSE - North Converged (m)	Mean RMSE - Up Converged (m)
Dual-frequency ionosphere-free (L1-L2)	29.451	0.014	0.005	0.020
Triple-frequency ionosphere-free	26.318	0.014	0.005	0.019
Mixed code-phase	26.831	0.013	0.005	0.019

Individual uncombined signals	27.036	0.014	0.005	0.019

Figure 1 shows, as an example, the PPP 3D positioning errors for the 24 hourly sessions at HOB2 using the traditional L1/L2 dual-frequency model. Figure 2 shows the positioning errors using the same data set but when using the triple-frequency low noise ionosphere-free model, whereas Figure 3 shows the result with the mixed code-phase model and Figure 4 shows the result for the individual uncombined model. Moreover, Figures 5-8 show the same plots for CEDU, whereas the plots for TIDB are given in Figures 9-12. The histograms for the convergence time and the RMSE East, North and Up are depicted in the Figures 13-16 for the solutions using the dual-frequency traditional PPP model, the triple-frequency low noise ionosphere-free model, the mixed code-phase model and the individual uncombined model, respectively. Comparing the distribution of the convergence time in these figures shows that most of the solutions from the triple-frequency model converged faster than the dual frequency case, with means between 26-27 minutes, compared to 29 minutes for the dual-frequency case. The RMSE values in East and Up are lower for most of the converged solutions that used the triple-frequency model.
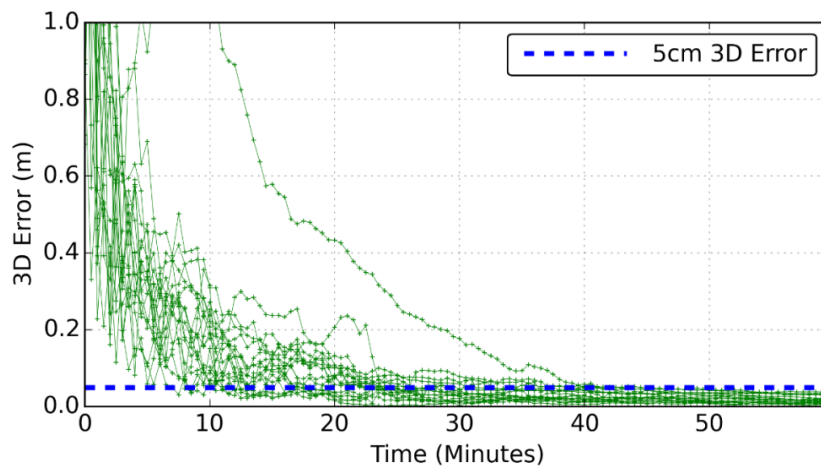
Figure 1: Dual-frequency (L1/ L2) ionosphere-free PPP 3D positioning errors for the 24 hourly solutions at HOB2.
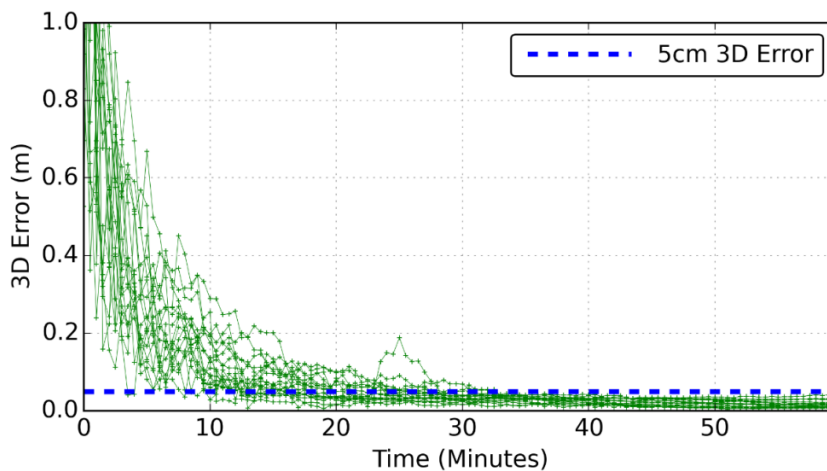
Figure 2: Triple-frequency ionosphere-free PPP 3D positioning errors for the 24 hourly solutions at HOB2.
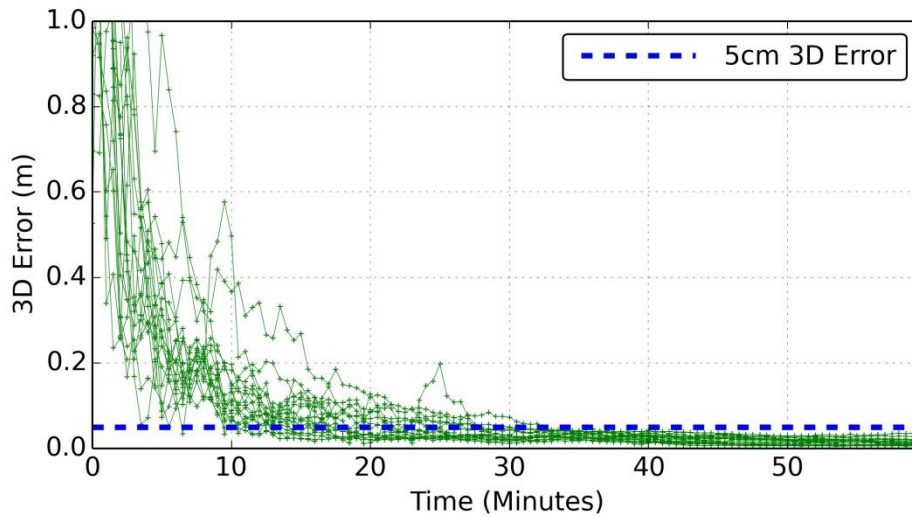
Figure 3: Mixed code-phase PPP 3D positioning errors for the 24 hourly solutions at HOB2.
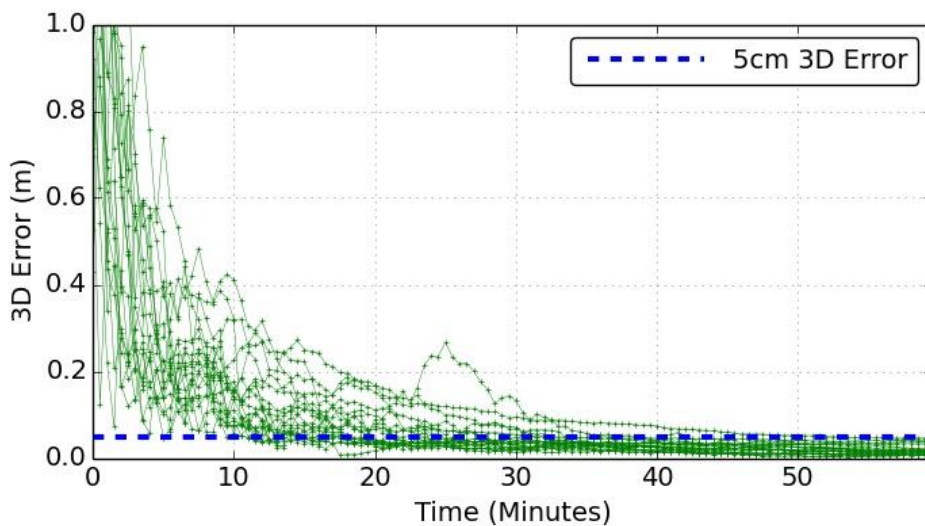
Figure 4: Individual uncombined signals PPP 3D positioning errors for the 24 hourly solutions at HOB2.
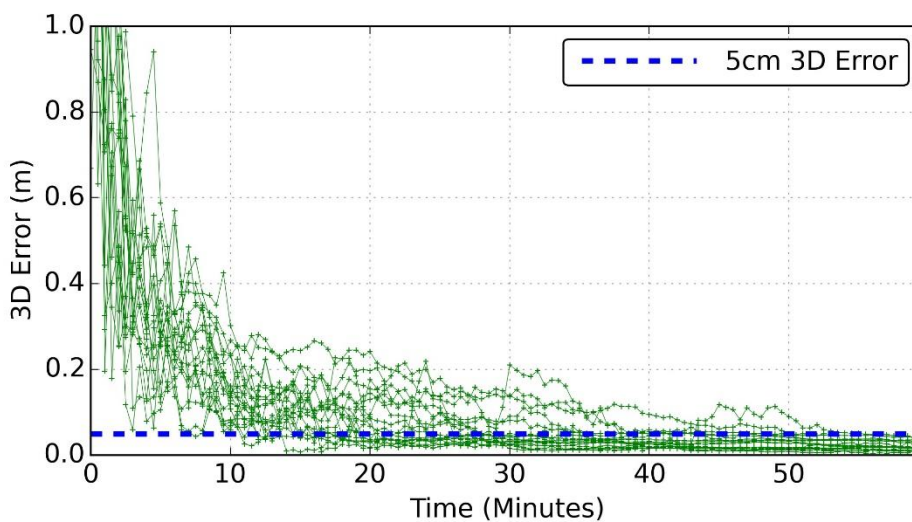
Figure 5: Dual-frequency (L1/ L2) ionosphere-free PPP 3D positioning errors for the 24 hourly solutions at CEDU.
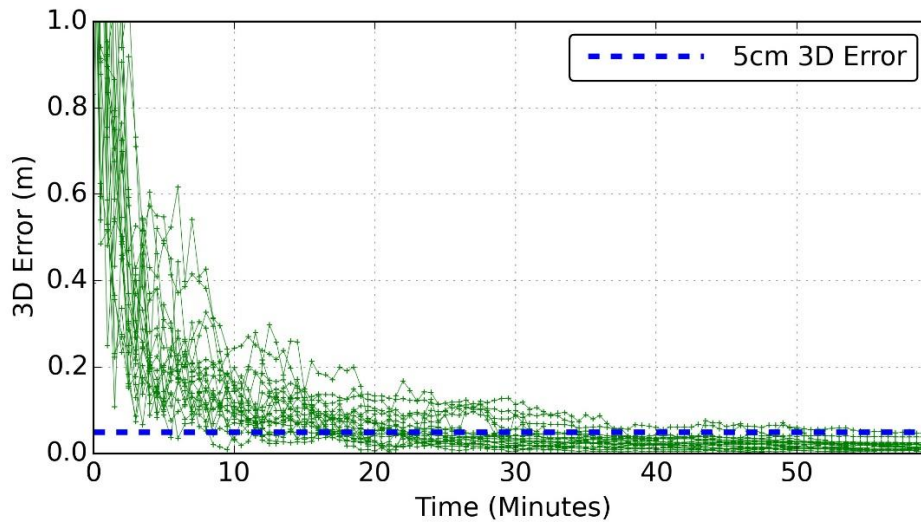
Figure 6: Triple-frequency ionosphere-free PPP 3D positioning errors for the 24 hourly solutions at CEDU.
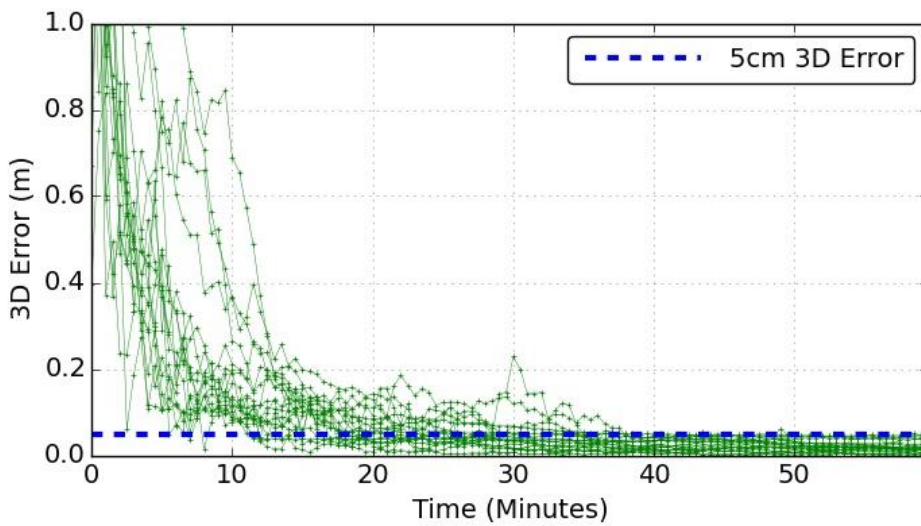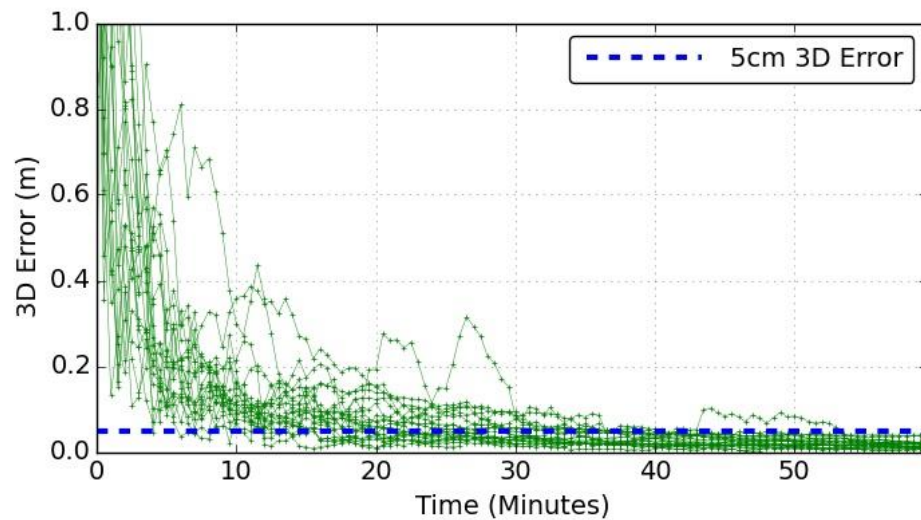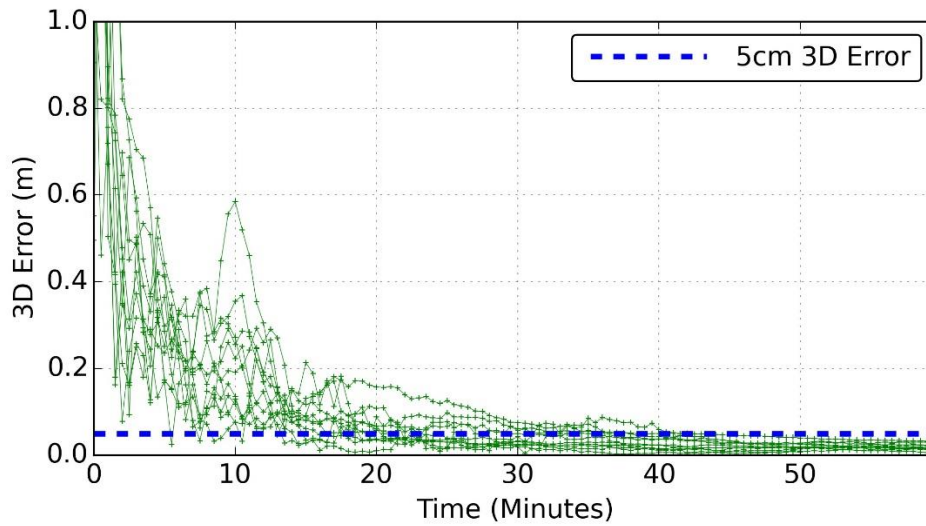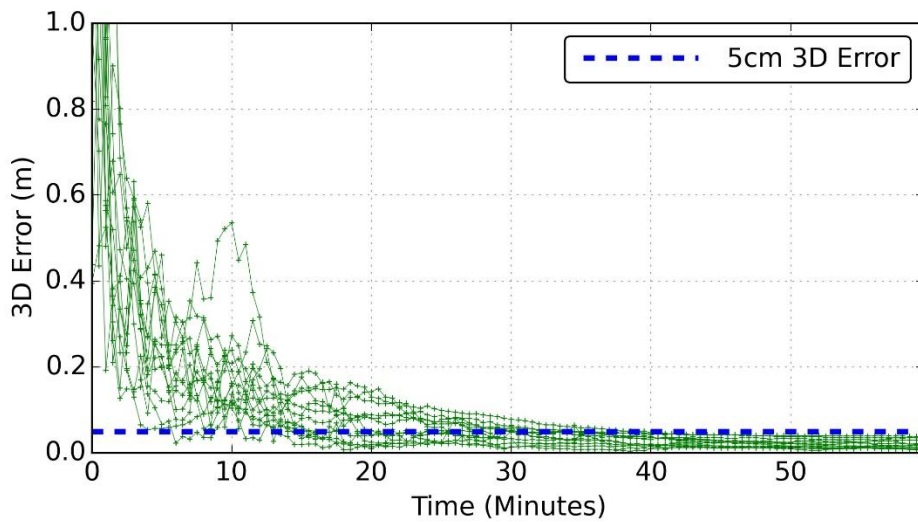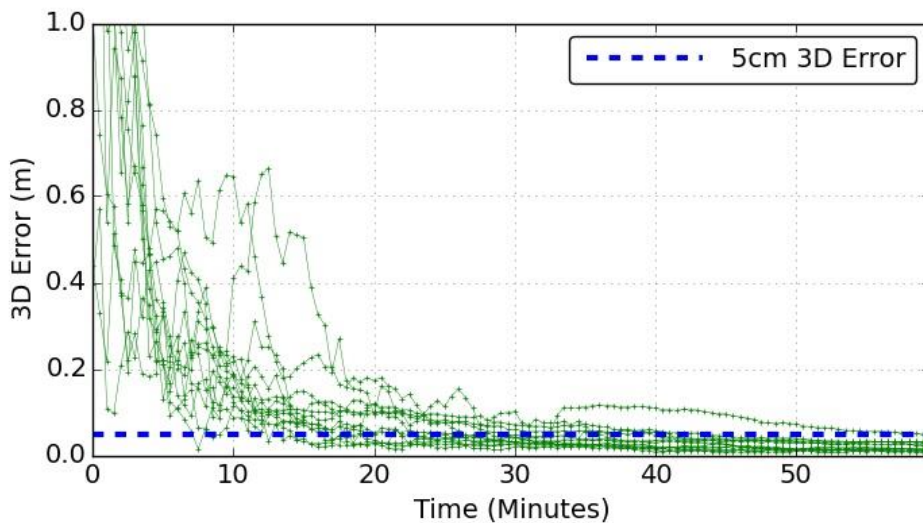

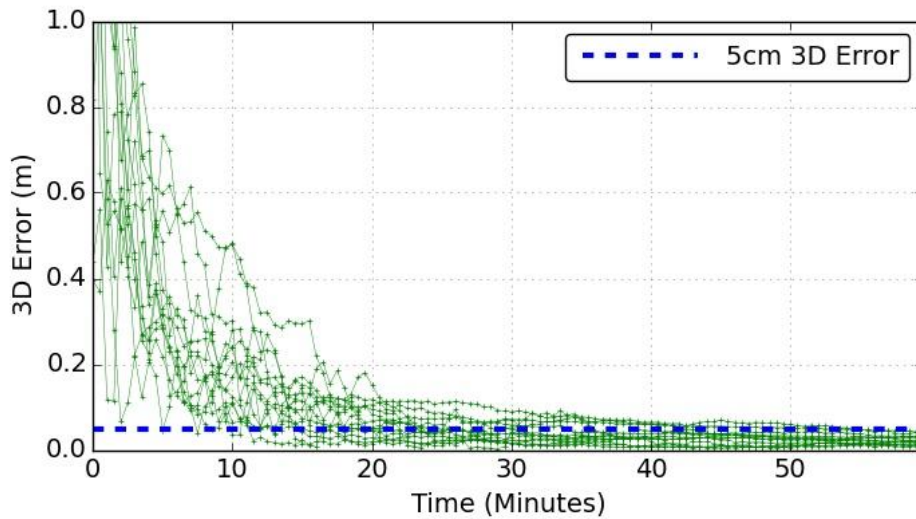Figure 7: Mixed code-phase PPP 3D positioning errors for the 24 hourly solutions at CEDU.

Figure 8: Individual uncombined signals PPP 3D positioning errors for the 24 hourly solutions at CEDU.

Figure 9: Dual-frequency (L1/ L2) ionosphere-free PPP 3D positioning errors for the 24 hourly solutions at TIDB.

Figure 10: Triple-frequency ionosphere-free PPP 3D positioning errors for the 24 hourly solutions at TIDB.

Figure 11: Mixed code-phase PPP 3D positioning errors for the 24 hourly solutions at TIDB.

Figure 12: Individual uncombined signals PPP 3D positioning errors for the 24 hourly solutions at TIDB.
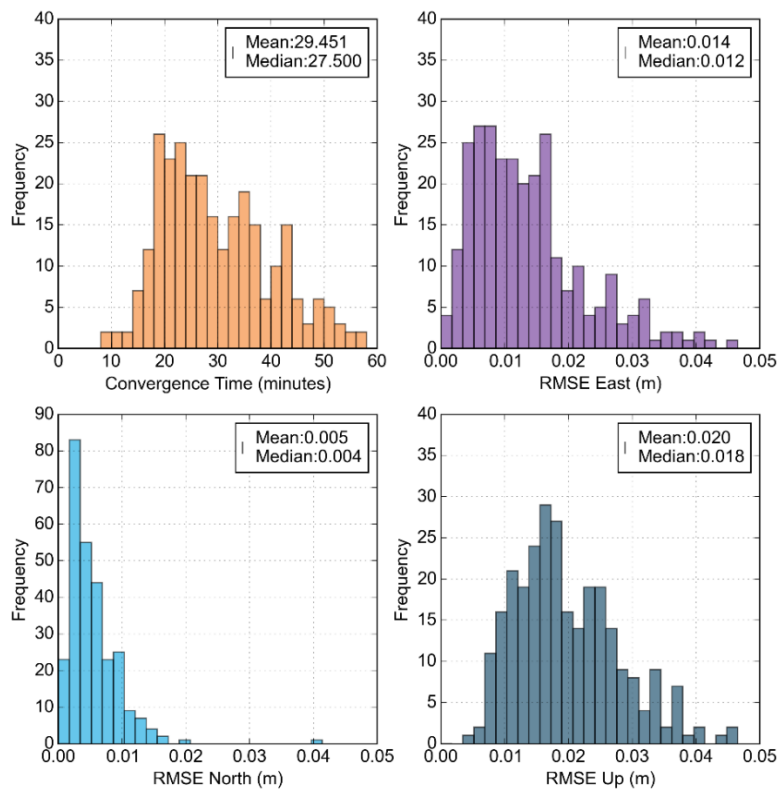

Figure 13: Histograms for the convergence time and the RMSE (in m) for East, North and Up obtained solutions using the L1/L2 dual-frequency traditional PPP model for all converged solutions. The mean and median of the histogram are given.
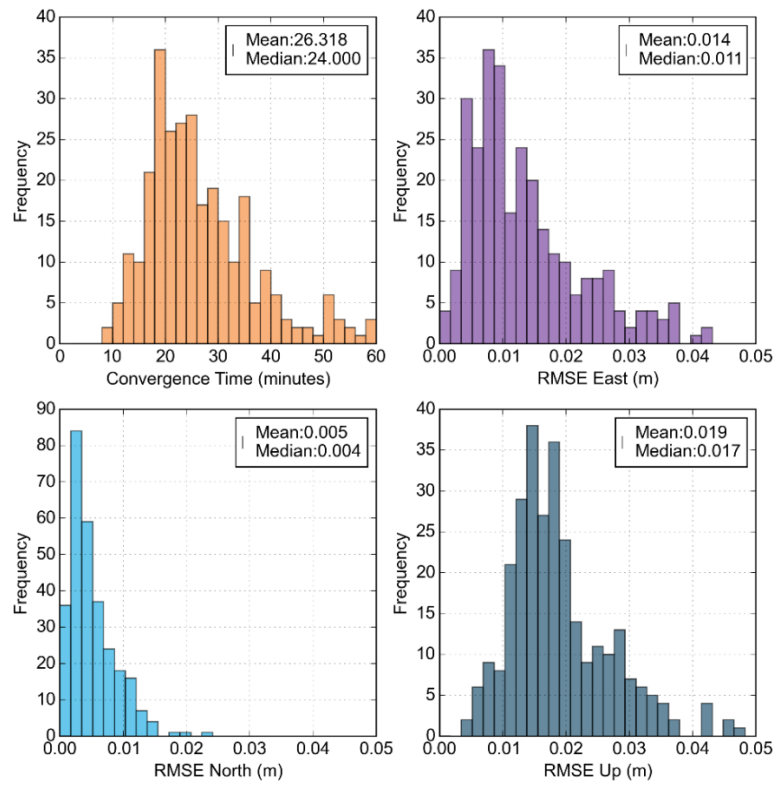
Figure 14: Histograms for the convergence time and the RMSE (in m) for East, North and Up obtained solutions using the low noise, ionosphere-free triple-frequency PPP model for all converged solutions. The mean and median are given.
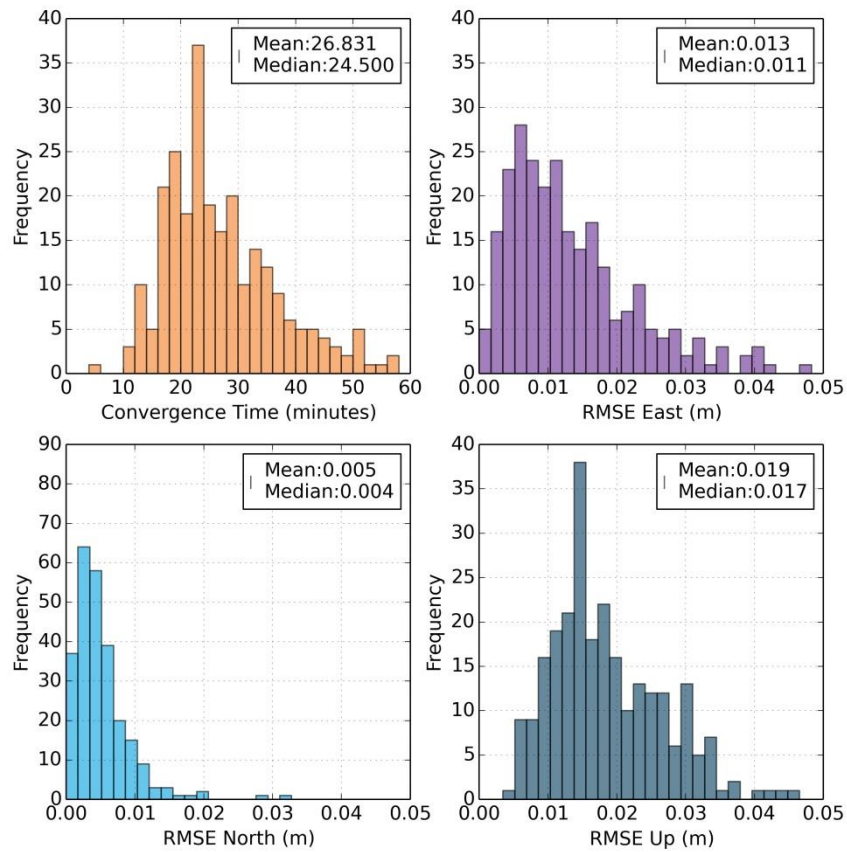
Figure 15: Histograms for the convergence time and the RMSE (in m) for East, North and Up obtained solutions using mixed code-phase PPP model for all converged solutions. The mean and median are given.
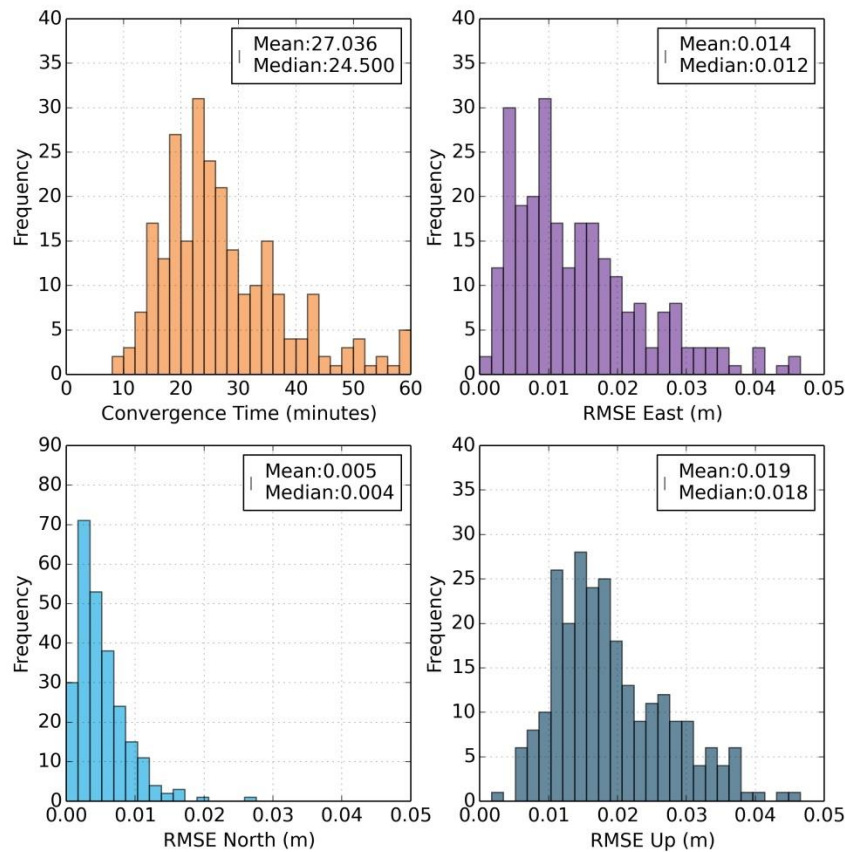
Figure 16: Histograms for the convergence time and the RMSE (in m) for East, North and Up obtained solutions using individual uncombined PPP model for all converged solutions. The mean and median are given.

Conclusion

In this contribution, three triple-frequency PPP models were presented for faster convergence of carrier-phase float ambiguities. In the first model, a new triple-frequency ionosphere-free linear combination was developed with minimum noise propagation and geometry preserving properties. The second proposed model used mixed code and carrier-phase linear combinations with two dual-frequency data, which also has the same properties. A third PPP model was also tested, that uses individual uncombined triple-frequency measurements.

These models were validated with several days of triple-frequency data and results were compared to the traditional dual-frequency model. It was shown that all three triple-frequency models had improved the solution convergence time required to achieve and maintain a 3D positional accuracy of 5cm, compared to the dual-frequency traditional PPP model. The triple-frequency code only and phase only ionosphere-free model, the mixed code and phase model and the individual uncombined model resulted in improvement of the convergence time by 11% (3.1 min), 9% (2.6 min) and 8% (2.4 min), respectively. The positioning accuracy after convergence for all triple-frequency algorithms was similar and showed marginal improvement at approximately 1mm, compared to the present dual-frequency model. The individual uncombined model with externally

provided ionosphere corrections can significantly improve convergence time to achieve 5cm 3D accuracy.

References

Banville, S. et al. 2014. Global and Regional Ionospheric Corrections for Faster PPP Convergence, Navigation, 61(2): 115-124.

Bisnath, S. and Gao, Y. 2009. Precise Point Positioning A Powerful Technique with a Promising Future, GPS World, April 2009.

Bohem, J. Werl, B. and Schuh, H. 2006. Troposphere mapping functions for GPS and VLBI from ECMWF operational analysis data, J Geophys Res 111(B02406).

Cocard, M. et al. 2008. A systematic investigation of optimal carrier-phase combinations for modernized triple-frequency GPS, J Geodesy, 82: 555-564.

Collins, P. et al. 2010. Undifferenced GPS ambiguity resolution using the decoupled clock model and ambiguity datum fixing. J Inst Navigat 57(2):123–135.

Davis, J.L. et al. 1985. Geodesy by radio interferometry: effects of atmospheric modelling errors on estimates of baseline length. Radio Sci 20(6):1593–1607.

Elsobeiey, M. 2015. Precise Point Positioning using Triple-Frequency GPS Measurements, The Journal of Navigation 68: 480-492.

El-Mowafy, A. Deo, M. and Rizos, C. 2016. On biases in precise point positioning with multi-constellation and multi-frequency GNSS data, Meas. Sci. Technol. 27(3), 035102.

El-Mowafy, A. 2014. GNSS Multi-frequency Receiver Single-Satellite Measurement Validation Method, GPS Solutions, 18(4), 553-561.

El-Mowafy, A. 2015. Estimation of Multi-Constellation GNSS Observation Stochastic Properties Using a Single-Receiver Single-Satellite Data Validation Method, Survey Review, 47(341), 99-108.

Gao, Y. and Shen, X. 2002. A New Method for Carrier Phase Based Precise Point Positioning, Navigation, 40(2): 109-116.

Ge, M. et al. 2008. Resolution of GPS carrier-phase ambiguities in precise point positioning (PPP) with daily observations. J Geodesy, 82(7):389–399

Geng, J. and Bock, Y. 2013. Triple-frequency GPS precise point positioning with rapid ambiguity resolution, J Geodesy, 87: 449-460.

Geng, J. et al. 2010. Rapid re-convergences to ambiguity-fixed solutions in precise point positioning. J Geodesy, 84(12):705–714.

GPS World 2016. 2016 State of the GNSS Industry. GPS World, September 2016: 41-46.

Guo, F. et al. 2016. Modelling and assessment of triple-frequency BDS precise point positioning. J. Geodesy.

Henkel, P. and Günther, C. 2008. Precise point positioning with multiple Galileo frequencies. In: Proceedings of the IEEE/ION symposium on position, location and navigation, Monterey, CA, 592–599

Laurichesse, D. et al. 2009. Integer ambiguity resolution on undifferenced GPS phase measurements and its application to PPP and satellite precise orbit determination. Navigation, 56(2):135–149

Montenbruck, O. Hauschild, A. and Steigenberger, P. 2014. Differential Code Bias Estimation using Multi-GNSS Observations and Global Ionosphere Maps, ION-ITM-2014, 27-29 January, San Diego, USA, 2014.

Montenbruck, O. et al. 2012. Apparent clock variations of the Block IIF-1 (SVN62) GPS satellite. GPS Solution, 16(3):303–313.

Prange, L. et al. 2012. MGEX data analysis at CODE – first Experiences, IGS Workshop, 23-27 July 2012, Olsztyn, Poland, 2012.

Richert, T. and El-Sheimy, N. 2007. Optimal linear combinations of triple frequency carrier phase data from future global navigation satellite systems, GPS Solution, 11(1):11-19.

Seepersad, G. and Bisnath, S. 2014. Reduction of PPP convergence period through pseudorange multipath and noise mitigation, GPS Solution, 19(3): 369-379.

Shi, J. et al. 2014. Local troposphere augmentation for real-time precise point positioning. Earth, Planets and Space 66(30), 2014.

Shi J. and Gao Y. 2014. A comparison of three PPP integer ambiguity resolution methods. GPS Solution, 18(4): 519-528.

Tegedor, J. and Øvstedal, O. 2014. Triple carrier precise point positioning (PPP) using GPS L5, Survey Review, 46(337): 288-297.

Tuka, A. and El-Mowafy, A. 2013. Performance Evaluation of Different Troposphere Delay Models and Mapping Functions, Measurement 46(2): 928–937.

Uhlemann, M. Ramatschi, M. and Gendt, G. 2012. GFZ's Global Multi-GNSS Network and First Data Processing Results, IGS Workshop, July 23-27 2012, Olsztyn, Poland.

Yuri, U. et al. 2011, GLONASS Modernisation, GPS World, 22(11), 4 pages.

Zhao, Q. et al. 2012. Initial results of precise orbit and clock determination for COMPASS navigation satellite system, J Geodesy, 87: 475-486.

Zumberge, J.F. et al. 1997. Precise point positioning for the efficient and robust analysis of GPS data from large networks. J Geophys Res 102(B3):5005–5017.

Appendix A

In this section, we provide the full derivation of the coefficients for the mixed code-carrier linear combination. Rearranging Eq. 24 gives:

$$\alpha_2 = 1 - \alpha_1 - \beta_1 - \beta_2 \tag{A1}$$

and substituting Eq. A1 into 23 and presenting in terms of the frequency multipliers results in:

$$\beta_1 = \frac{k_2\alpha_1 + k_1 - k_1\alpha_1 - 2k_1\beta_2}{k_1 + k_2} \tag{A2}$$

Squaring Eq. A2 gives

$$\beta_1^2 = \frac{(k_2\alpha_1 + k_1 - k_1\alpha_1)^2 - 4k_1\beta_2(k_2\alpha_1 + k_1 - k_1\alpha_1) + 4k_1^2\beta_2^2}{(k_1 + k_2)^2} \tag{A3}$$

and substituting Eq. A2 into A1 we have:

$$\alpha_2 = \frac{k_2 - 2k_2\alpha_1 + \beta_2(k_1 - k_2)}{k_1 + k_2} \tag{A4}$$

and its squaring gives:

$$\alpha_2^2 = \frac{k_2^2(1 - 2\alpha_1)^2 + 2k_2\beta_2(1 - 2\alpha_1)(k_1 - k_2) + \beta_2^2(k_1 - k_2)^2}{(k_1 + k_2)^2} \tag{A5}$$

Substituting Eq. A3 and Eq. A5 into Eq. 25 results in a quadratic equation $A\beta_2^2 + B\beta_2 + C = 0$ where β_2 and ϵ are the unknown variables. The constants A, B, and C are:

$$A = a^2(k_1 + k_2)^2 + (k_1 - k_2)^2 + 4a^2k_1^2 \tag{A6}$$

$$B = 2k_2(1 - 2\alpha_1)(k_1 - k_2) - 4a^2k_1(k_2\alpha_1 + k_1 - k_1\alpha_1) \tag{A7}$$

$$C = (k_1 + k_2)^2\alpha_1^2 + k_2^2(1 - 2\alpha_1)^2 + a^2(k_2\alpha_1 + k_1 - k_1\alpha_1)^2 - (k_1 + k_2)^2\epsilon^2 = C_0 - (k_1 + k_2)^2\epsilon^2 \tag{A8}$$

where $C_0 = (k_1 + k_2)^2\alpha_1^2 + k_2^2(1 - 2\alpha_1)^2 + a^2(k_2\alpha_1 + k_1 - k_1\alpha_1)^2$ is a constant and C is calculated directly in analogy with Eq. 19. The noise amplification factor in the combination ϴ12 is evaluated by:

$$\epsilon = \sqrt{\frac{C_0 - C}{(k_1 + k_2)^2}} = \frac{\sqrt{C_0 - C}}{k_1 + k_2} \tag{A9}$$

Since α_1 is present as a variable in Eq. A7, its direct analytical solution at a minimum noise is obtained by assigning the first derivation of Eq. A9 with respect to α_1 to 0, such that:

$$\epsilon'(\alpha_1) = \frac{C_0'(\alpha_1) - C'(\alpha_1)}{2(k_1 + k_2)\sqrt{C_0 - C}} \tag{A10}$$

The minimum value of α_1 occurs when the above Eq. A10 (its numerator) is equated to 0, which results in:

$$C_0'(\alpha_1) - C'(\alpha_1) = 0 \tag{A11}$$

where:

$$C_0'(\alpha_1) = X_1\alpha_1 + X_2 \tag{A12}$$

with

$$X_1 = \alpha_1(2(k_1 + k_2)^2 + 8k_2^2 + 2a^2(k_2 - k_1)^2) \tag{A13}$$

and

$$X_2 = -4k_2^2 + 2a^2(k_2 - k_1)k_1 \tag{A14}$$

$C_0'(\alpha_1)$ is evaluated as:

$$C_0'(\alpha_1) = \frac{2X_3}{A}(\alpha_1X_3 + X_5) \tag{A15}$$

with

$$X_3 = -2k_2(k_1 - k_2) - 2a^2k_1k_2 - 2a^2k_1^2 \tag{A16}$$

and

$$X_5 = k_2(k_1 - k_2) - 2a^2k_1^2 \tag{A17}$$

The variable A, which is evaluated using Eq. A6, is used to obtain a solution for α_1 as:

$$\alpha_1 = \frac{2X_3X_5 - AX_2}{AX_1 - X_3^2} \tag{A18}$$

The corresponding value for β_2 is calculated as $\beta_2 = -B/2A$; whereas α_2 and β_1 are calculated using Eq. A4 and A2, respectively.